Inorganic Chemistry

pubs.acs.org/IC Article

Developing Iron–Nickel Bimetallic Oxides with Nanocage Structures As High-Performance Bifunctional Catalysts via the Ensemble Effect from Nitrogen Sources

Taeoh Kang, Kwanwoo Kim, and Jooheon Kim*

Cite This: *Inorg. Chem.* 2021, 60, 7490–7497 Read Online

ACCESS | Metrics & More | Article Recommendations | Supporting Information

ABSTRACT: Metal-air batteries will serve as renewable and ecofriendly energy-storage systems in the future because of their high theoretical energy-density performance and unlimited resources, using oxygen as fuel materials compared with commercial lithium-ion batteries. However, the unsuitable inactive reactions at the air–electrode interface (the oxygen reduction reaction and the oxygen evolution reaction) in the metal–air battery are major challenges. In this study, we report nitrogen (N)-doped iron (Fe) and nickel (Ni) bimetallic catalysts with a hollow structure (Fe–Ni nanocage) as outstanding bifunctional catalysts, which have not been reported previously. The open structure in the catalysts simultaneously has an active inner cavity and an outer shell; catalysts have a high active surface area, resulting in remarkable electrochemical performance. Furthermore, the electron transfer phenomenon due to the "ensemble effect" generates a higher catalyst activation. Nitrogen has a higher electronegativity than the metal cations, so doped nitrogen sources draw the electron into iron and nickel cations, and the deprived oxidation state of the metal cations accelerates the electrocatalytic performance.

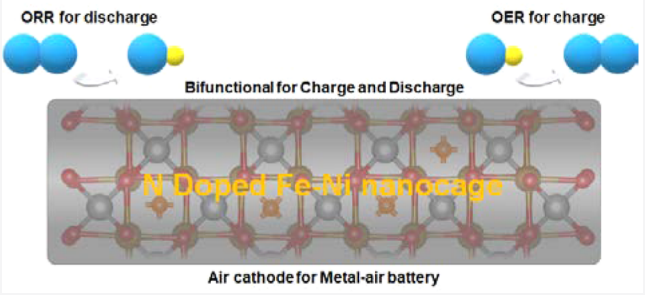

1. INTRODUCTION

Recently, increasing energy demands have prompted an enormous amount of research that aims to develop renewable energy storage and conversion systems with ecofriendly characteristics and a high energy density such as the metal–air battery, which draws much attention as a next-generation energy storage device.[1−7] Metal–air batteries, which consist of an air cathode, are operated by oxygen reactivity and have a high theoretical energy density.[8,9] However, their kinetic sluggishness and high overpotential are significant challenges. Numerous studies have selected noble metals such as platinum (Pt), ruthenium (Ru), and iridium (Ir) as attractive catalyst candidates to address these challenges because of their low overpotentials and high electrochemical properties.[10−13] However, noble metals are expensive due to their scarcity and have poor durabilities because of corrosion and agglomeration.[14] Consequently, the development of substitute materials for noble metals is the most promising approach to achieve a low cost and high durability for the oxygen reduction reaction (ORR) and oxygen evolution reaction (OER).

To substitute the high-cost noble metal, 3d transition metal-based catalysts, such as cobalt (Co), iron (Fe), and nickel (Ni), have been attracting attention due to their proper electrocatalytic activities and low prices.[15] Furthermore, designing a unique structure or doping heteroatoms (B, N, P, and S) into catalysts are acceptable strategies.[16−19] The doped heteroatom modulates the atomic charge density and spin-charge density of the catalyst materials, which result from differences in electronegativity.[20] Consequently, the increased adsorption energy with oxygen on the catalyst surface increases the reactivity with oxygen, which is desirable for the ORR and OER.[21] Moreover, heteroatoms with high electron negativities cause the electron transfer phenomenon, where doped heteroatoms withdraw the electrons from metal centers. This phenomenon is called the "ensemble effect" and generates a synergistic effect for high electrocatalyst performance.[22−24]

Among the 3d transition metals, Ni has been researched in the electrochemical catalyst field as a promising material for the ORR and OER.[25−29] However, despite many attempts to overcome the low overpotentials of non-noble metals, several challenges remain. Previous studies suggested that the electrochemical catalytic activities of transition metal-based bimetallic catalysts are higher than those of their single-metal counterparts. Furthermore, the Ni receives the influence of positive sides from the Fe metal for the Fe–Ni bimetallic phase.[30−36] Consequently, the Fe–Ni bimetallic phase has various advantages for bifunctional electrocatalysts.

Received: March 14, 2021
Published: May 4, 2021

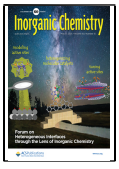

https://doi.org/10.1021/acs.inorgchem.1c00782
Inorg. Chem. 2021, 60, 7490–7497

Scheme 1. (a) Schematic Representation of the Simple Reduction Process for Fe−Ni Nanocage Synthesis

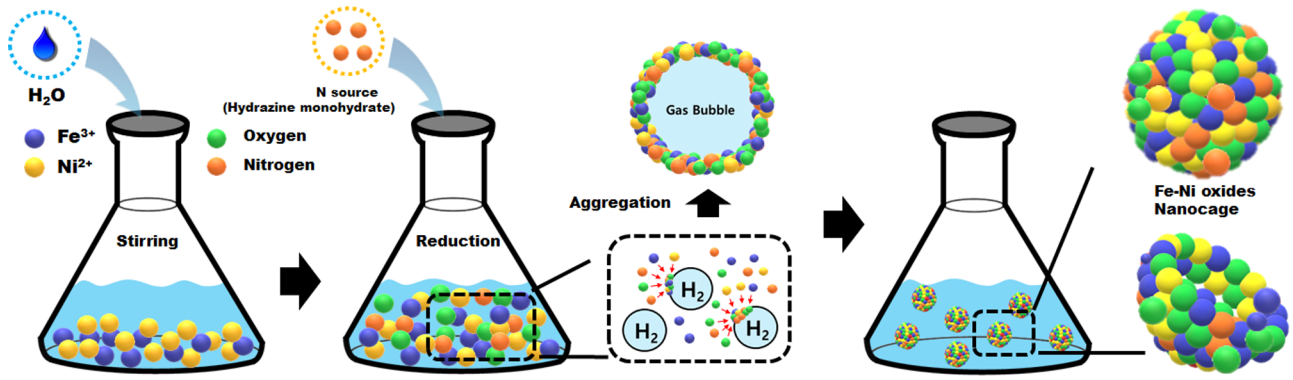

Furthermore, the design of unique structures with a high surface area is an important part of developing electrochemical catalysts for the application of new energy conversion and storage systems to overcome energy demands and identify green energy sources. From this point of view, designing an open structure, such as hollow or cage structures with empty core sites and shell walls, is a suitable strategy to enhance the electrochemical performances because both the inner and outer sites of the shell can play a role as active centers during ORR and OER processes. Utilization efficiency (UE) is another factor to decide the electrochemical performances.[37] In the cases of hollow and cage structures, the UE of the active metal center is higher than that of a normal particle due to the empty core. Based on the previous research results, changing to open structures increases the UE more than threefold.[37]

In this study, we fabricated nitrogen (N)-doped iron (Fe) and nickel (Ni) bimetallic catalysts with nanocage structures (Fe−Ni nanocage) as new electrochemical catalysts to design a unique structure with many synergistic effects based on the bimetallic phase and "ensemble effect". The nanocage structures are aggregated with the hydrogen bubble as templates, which occurs during the reduction reaction by a reduction agent. Well-synthesized iron and nickel bimetallic catalysts have empty cores and 10 nm thick shells. The crystalline Fe−Ni nanocage demonstrates outstanding bifunctional ORR and OER performances, which are crucial reactions for the air−electrode surface of the metal−air battery.

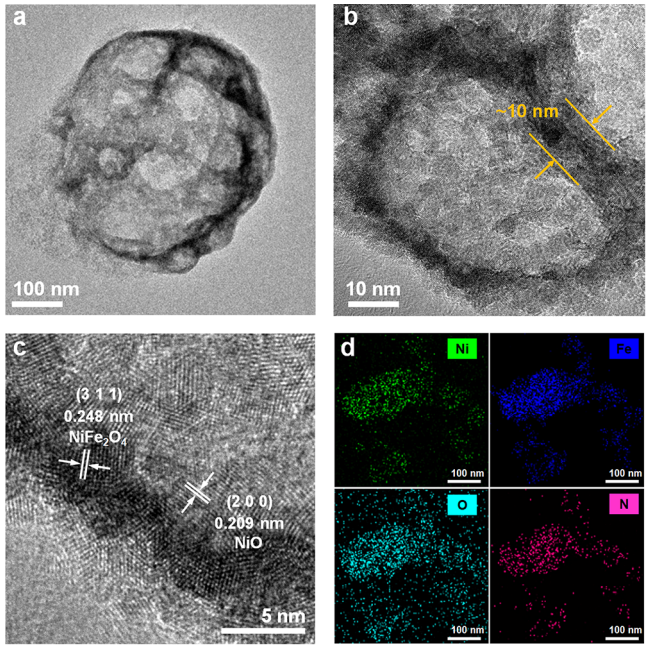

Figure 1. (a) Low-magnification FE-TEM image of an Fe−Ni nanocage. (b) Middle-magnification FE-TEM image of an Fe−Ni nanocage. (c) High-magnification FE-TEM image of an Fe−Ni nanocage. (d) EDS element mapping images of an Fe−Ni nanocage.

2. RESULTS AND DISCUSSION

2.1. Characterization. The fabrication process and proposed mechanism used to synthesize the Fe−Ni nanocage is depicted in Scheme 1. $FeCl_3{\cdot}6\ H_2O$, $Ni(NO_3)_2{\cdot}6H_2O$, and melamine were used as Fe, Ni, and nitrogen sources, respectively, to synthesize the Fe−Ni nanocage catalyst. The nanocage shape of the catalyst was combined with Fe and Ni cations as bimetallic oxides through a simple reduction process using a hydrazine monohydrate ($H_4N_2{\cdot}H_2O$) reduction agent. The generated hydrogen bubble used the template to form the nanocage structure. The inner cavity and outer shell, which have high active surface areas, can operate simultaneously during the electrochemical process, resulting in outstanding electrochemical properties.

Field-emission transmission electron microscopy (FE-TEM) results in Figures 1 and S1 demonstrate the nanoscale morphology and open structure of the catalyst materials. FE-TEM images show that catalysts have a nanocage morphology and about a 10 nm thick shell (Figure 1a and b). In addition, as shown in Figure 1c, the lattice interlayer distances of 0.232, 0.22, and 0.218 nm correspond to the (200) and (311) diffraction planes of nickel oxide (NiO) and bimetallic Fe−Ni oxide ($NiFe_2O_4$), respectively.[38,39] Figure 1d presents the EDS mapping images for the Fe−Ni nanocage, showing the uniform distribution of Ni, Fe, O, and N throughout the catalysts. FE-TEM images display the well-defined cage-like structure with a nanoscale size, which has an inner cavity and a bimetallic lattice in the outer shell.

The X-ray diffraction (XRD) patterns in Figure 2a−c were used to identify the lattice structures of the Fe−Ni nanocage. In the high-resolution FE-TEM image in Figure 1c, the Fe−Ni nanocage catalysts exhibit a distinctive lattice fringe by the metal oxide structure. Figure 2a−c exhibits the X-ray diffraction (XRD) patterns of the Fe−Ni nanocage with different ratios, showing that the catalyst consists of NiO and $NiFe_2O_4$ (JCPDS card nos. 47-1049 for NiO and 54-0964 for $NiFe_2O_4$). As the ratio of Fe decreases, the peaks corresponding to NiFe2O4 decrease, demonstrating that Ni

https://doi.org/10.1021/acs.inorgchem.1c00782
Inorg. Chem. 2021, 60, 7490−7497

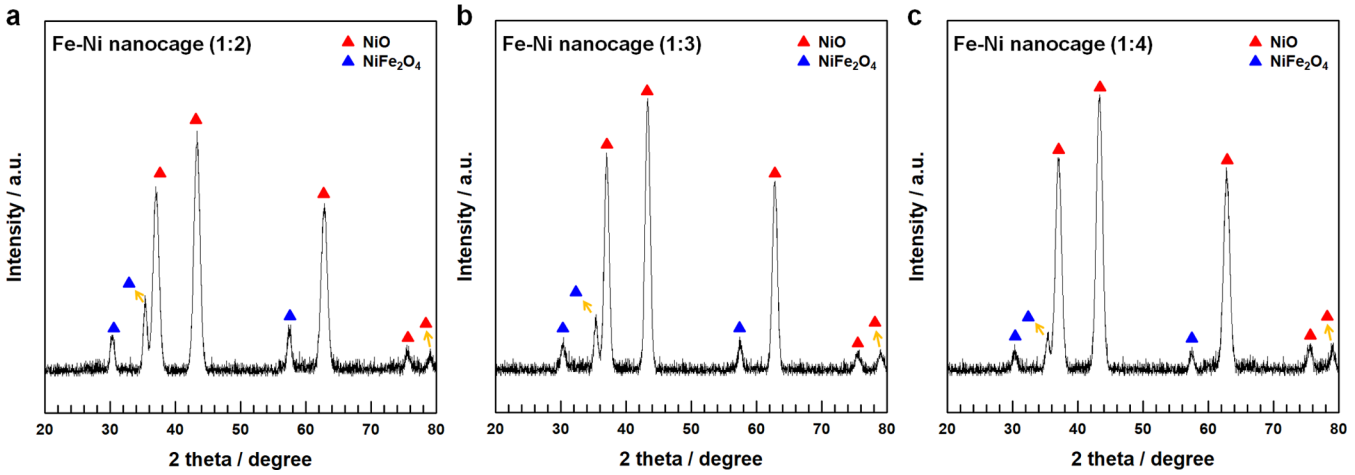

Figure 2. XRD patterns for Fe−Ni nanocages with ratio of (a) 1:2, (b) 1:3, and (c) 1:4.

and Fe ions are well dispersed in the lattice of the nanocage structure. An X-ray photoelectron spectroscopy (XPS) survey spectrum was used to characterize the composition of the Fe−Ni nanocage catalyst. As shown in Figure S2, the survey spectrum of the Fe−Ni nanocage shows that Fe, Ni, and O species compose the nanocage catalysts, and N species are successfully doped in the Fe−Ni nanocage.

To examine the chemical bonding and environment of the Fe−Ni nanocage, XPS peaks of Ni 2p, Fe 2p, O 1s, and N 1s were analyzed (Figure 3). Figure 3a shows the high-resolution Ni 2p spectrum of the Fe−Ni nanocage. For the Fe−Ni nanocage, the major Ni $2p_{1/2}$ and Ni $2p_{3/2}$ peaks were observed at approximately 856 and 874 eV, respectively, which are related to the Ni^{2+} state of NiO and $NiFe_2O_4$. Interestingly, the peaks corresponding to Ni^{2+} were slightly increased to higher binding energies compared to those of pure NiO. This phenomenon is called the "ensemble effect" and occurs due to the existence of N species. Other two peaks at around 862 and 880 eV are attributed from Ni 2p satellite peaks. In Figure 3b, the high-resolution Fe $2p_{1/2}$ spectrum was composed of Fe^{2+}, Fe^{3+}, and satellite peaks.[40] The major peak at around 711.6 eV arose from Fe^{3+} in $NiFe_2O_4$.[39] During the synthesis of the Fe−Ni nanocage, a small amount of Fe ions substituted the Ni ions at $NiFe_2O_4$, leading to the Fe^{2+} peak at around 710.3 eV in high-resolution Fe 2p spectrum.[41] The high-resolution O 1s spectrum is shown in Figure 3c. As shown in the O 1s spectrum, the O species in the Ni−Fe nanocage are composed of lattice oxygen in the metal oxide and H−O−H in adsorbed water molecules.[42−44] Figure 3d shows the deconvoluted XPS N 1s spectrum, which is composed of two main peaks. Two peaks correspond to the Ni oxide lattice at around 396.5 eV and N−O at around 400.3 eV.[45] The XPS results are accordance with the high-resolution FE-TEM image in Figure 1c and the XRD pattern in Figure 2b, ensuring that the nanocage catalyst is composed of NiO and $NiFe_2O_4$.

The slightly higher oxidation state of the metal in catalysts due to N doping, called the "ensemble effect", enable catalytic intermediates to form on the catalysts and lower the energy barrier of formation to the catalytic intermediates.[14−16] Additionally, the nanocage-shaped property enlarges the active surface area in contact with electrolyte. To test the electrochemical properties, we used some equipment and demonstrated the superior bifunctional activities.

2.2. Electrochemical Activity Measurements. An analysis of the LSV curve must be performed to evaluate the ORR and OER properties of the Fe−Ni nanocage. The ORR activities (E_{onset}, $E_{half\text{-}wave}$, and $J_{limited}$) and OER activity (E_{onset} and $E_{j:10}$ mA/cm^2) of the catalytic materials were tested with rotating disk electrode (RDE) equipment in an O_2- and N_2-saturated 0.1 M KOH solution at a 1600 rpm rotation speed and a 10 mV/s scan rate. To discover the best ratio of Fe to Ni, Fe−Ni nanocage catalysts with various ratios were synthesized, and electrochemical tests were conducted. First, electrochemical performances of N-NiO (no Fe content) and pure NiO (purchased from sigma Aldrich, <50 nm, 99.8 trace metals basis) were analyzed to confirm the ensemble effect and the nanocage-shape property (Figure S3). The N-NiO nanocage showed a better electrocatalytic performance than that of pure NiO, demonstrating that the morphology of the nanocage and ensemble effects from the N species improved the catalytic activities in both the OER and the ORR. Figure 4a illustrates the LSV curves of various Fe−Ni nanocages (Fe:Ni ratios of 1:2, 1:3, and 1:4) in a potential range from 1.1 to 0 V (vs RHE) to compare the ORR performance. The Fe−Ni nanocage (ratio of 1:3) shows favorable ORR performances, which have the lowest onset potential (0.89 V versus RHE) and the highest limiting current density of −5.917 mA/cm^2. Accordingly, the electrochemical properties of the Fe−Ni nanocage (ratio of 1:3) are superior to those of nanocages with other ratios (1:2 and 1:4). The electron transfer number is an important factor to estimate the ORR activity. To calculate the electron transfer number, LSV curves of each catalyst were recorded at different revolutions rotation speeds (rpm) (Figure S4). The slopes of Koutecky−Levich (KL) plots at different potentials are the electron transfer numbers during ORR (Figure S5). The Fe−Ni nanocage (ratio of 1:3) exhibits a higher electron transfer number (3.59−3.73) than those of Fe−Ni nanocages with other ratios (1:2 and 1:4), indicating favorable four-electron transfer during the ORR process (Figure 4b). Figure 4c also illustrates the electrochemical performance of various Fe−Ni nanocages (Fe:Ni ratio, 1:2, 1:3, and 1:4) in a potential range from 1.2 to 2.0 V (vs RHE; OER properties). The OER performance also demonstrated the highest activity of 1.68 V (vs RHE), achieving a current density of 10 mA/cm^2 for the Fe−Ni nanocage (ratio of 1:3) and revealing that the 1:3 ratio of Fe:Ni is the optimal point based on its outstanding electrochemical properties. To further

https://doi.org/10.1021/acs.inorgchem.1c00782
Inorg. Chem. 2021, 60, 7490−7497

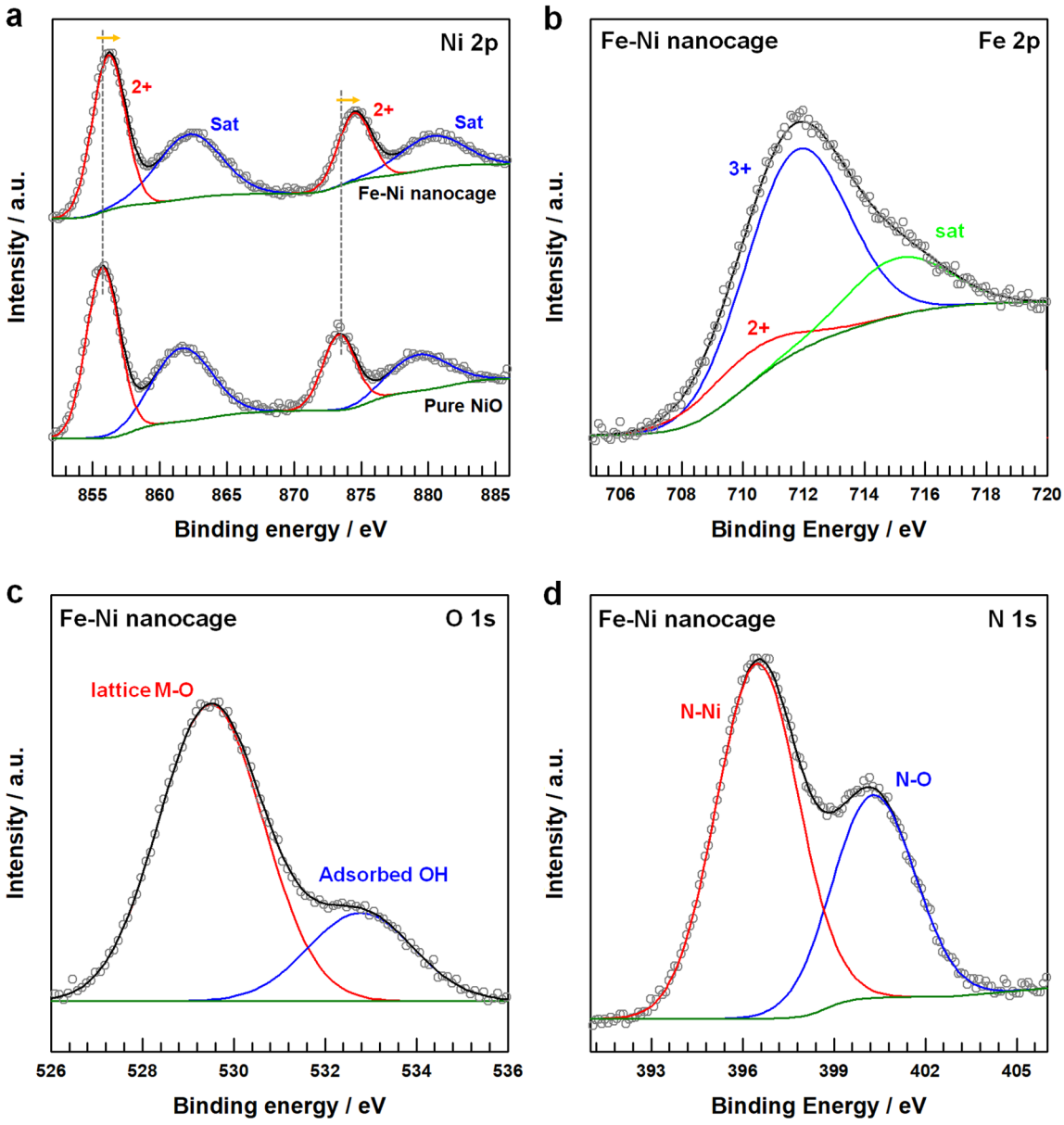

Figure 3. (a) High-resolution XPS Ni 2p XPS spectra of an Fe−Ni nanocage and pure NiO. (b) High-resolution XPS Fe 2p XPS spectrum of an Fe−Ni nanocage. (c) High-resolution XPS O 1s XPS spectrum of an Fe−Ni nanocage. (d) High-resolution XPS N 1s XPS spectrum of an Fe−Ni nanocage.

estimate the OER kinetics, Tafel plots were fitted by using LSV curves, and tafel slopes were calculated as shown in Figure 4d. The decrease in the Tafel slope expressed the enhanced OER kinetics, and from this it was confirmed that the Fe−Ni nanocage (ratio of 1:3) had the highest OER kinetics. The double-layer capacitance of the Fe−Ni nanocage (1:3) was calculated using the CV curves in the nonfaradic current region, as shown in Figure S6. To elucidate the superior OER activities, electrochemical impedance spectroscopy (EIS) was conducted (Figure 4e). The Fe−Ni nanocage with a ratio of 1:3 showed a smaller diameter than the other ratios (1:2 and 1:4), suggesting low charge-transfer resistance during the OER process.

Figure 5 illustrates the bifunctional properties of the Fe−Ni nanocage (ratio of 1:3) compared with those of the noble metal platinum and iridium catalysts (Pt/C and Ir/C, respectively). LSV curves for the Fe−Ni nanocage (ratio of 1:3), Pt/C, and Ir/C are shown in Figure 5a. For both the ORR and OER properties, the Fe−Ni nanocage (ratio of 1:3) had lower electrocatalytic activities than those of Pt/C for ORR and those of Ir/C for OER. To use them as catalysts at the air−electrode interface of the metal−air battery, however, the lower potential values between the ORR at a current density of −3 mA/cm^2 and the OER at a current density of 10 mA/cm^2 are desirable. As shown in Figure 5b, the difference between the ORR and OER potentials of the Fe−Ni nanocage (ratio of 1:3) is the lowest among the comparative group, demonstrating its excellent bifunctional electrocatalytic activities.

Durability and stability are crucial for the commercialization of electrocatalysts. A cycling test was performed using an RDE system to compare the durabilities of the Fe−Ni nanocage (ratio of 3:1) and the catalysts. Figure 6 illustrates the ORR and OER performances both initially and after 2000 fast cycles

https://doi.org/10.1021/acs.inorgchem.1c00782
Inorg. Chem. 2021, 60, 7490−7497

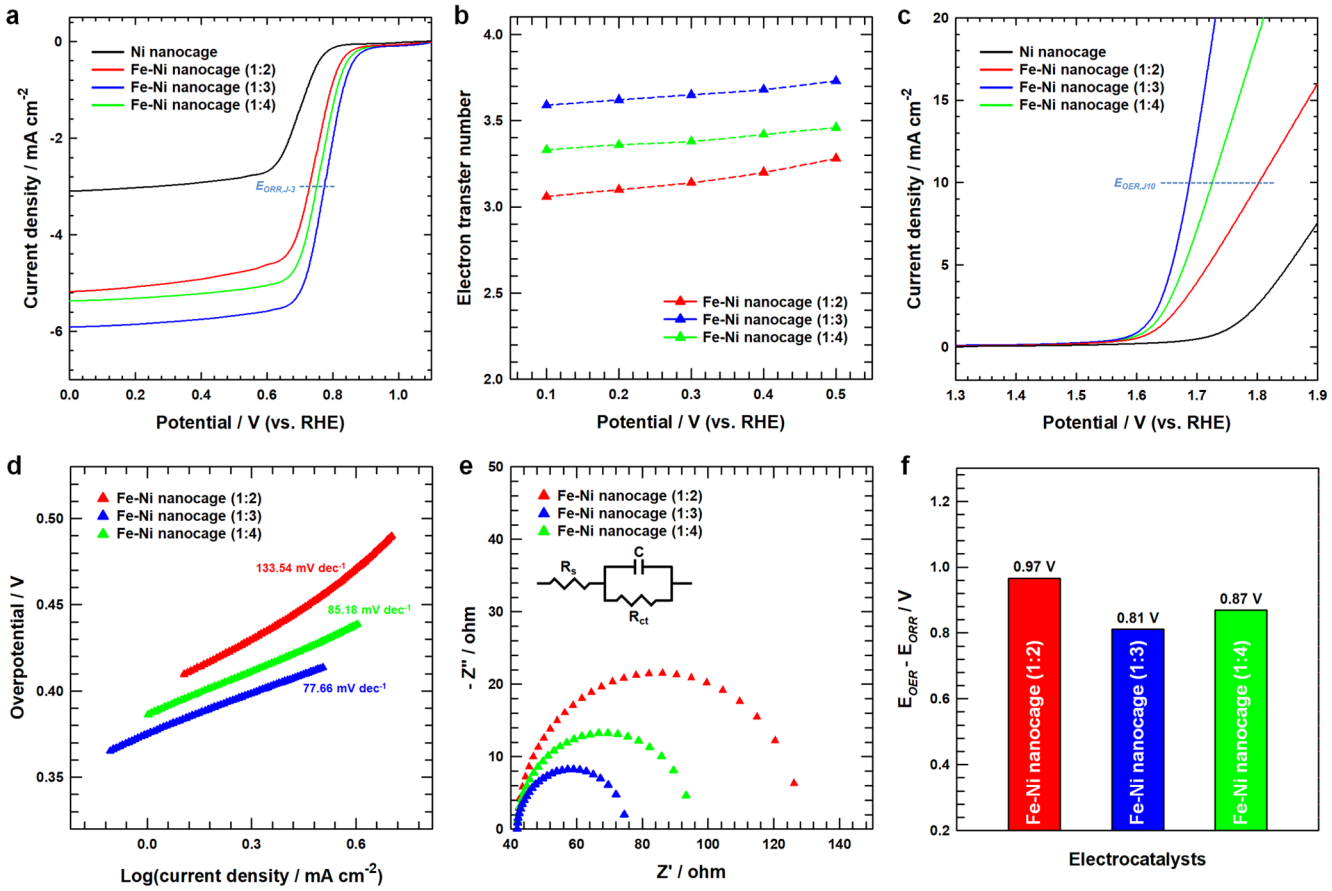

Figure 4. (a) LSV curves for the ORR of Fe−Ni nanocages with various Fe:Ni ratios (1:2, 1:3, an 1:4) in O_2-saturated 0.1 M KOH with a rotation rate of 1600 rpm. (b) Electron transfer number of Fe−Ni nanocages with various Fe:Ni ratios (1:2, 1:3, an 1:4) at different potentials (0.1−0.5 V versus RHE). (c) LSV curves for the OER of Fe−Ni nanocages with various Fe:Ni ratios (1:2, 1:3, an 1:4) in N_2-saturated 0.1 M KOH with a rotation rate of 1600 rpm. (d) Tafel plots for Fe−Ni nanocages with various Fe:Ni ratios (1:2, 1:3, and 1:4). (e) Nyquist plots for Fe−Ni nanocages with various Fe:Ni ratio (1:2, 1:3, and 1:4). (f) Bar plots for the comparison of $E_{OER} - E_{ORR}$ of Fe−Ni nanocages with different ratios.

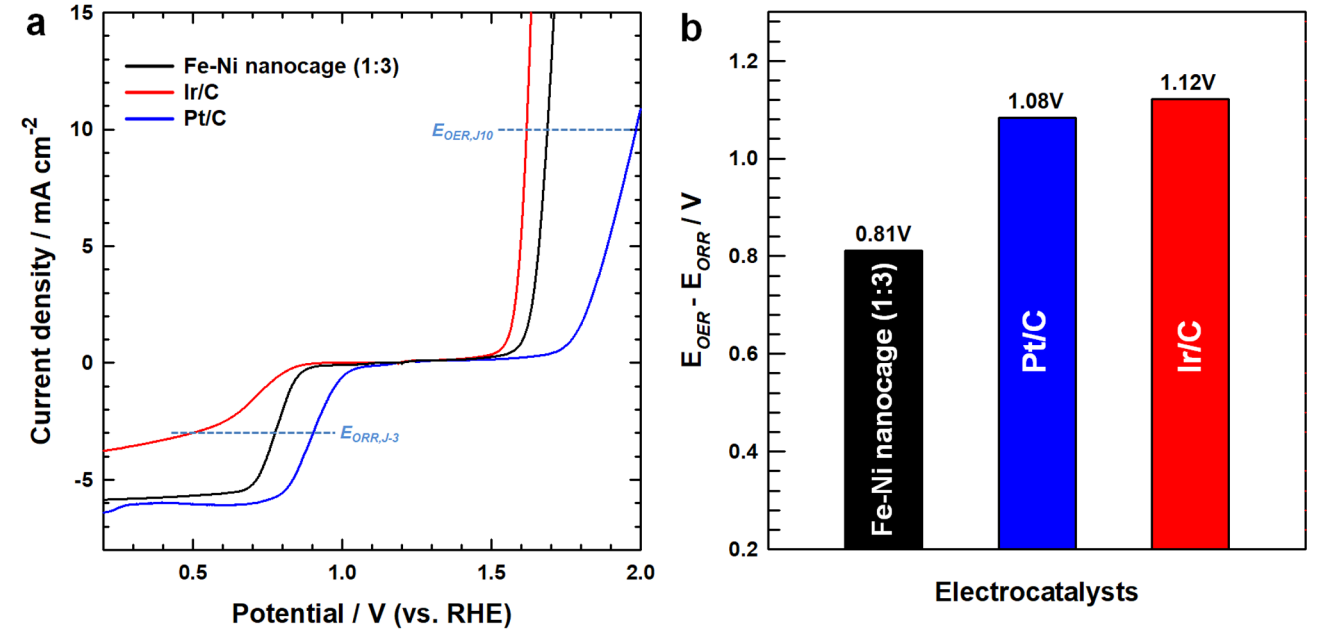

Figure 5. (a) The overall LSV curves of an Fe−Ni nanocage (ratio of 1:3) and Pt/C and Ir/C catalysts within the ORR and OER potential window. (b) Bar plots comparing the air−electrode activity of an Fe−Ni nanocage (ratio of 1:3), Pt/C, and Ir/C.

https://doi.org/10.1021/acs.inorgchem.1c00782
Inorg. Chem. 2021, 60, 7490−7497

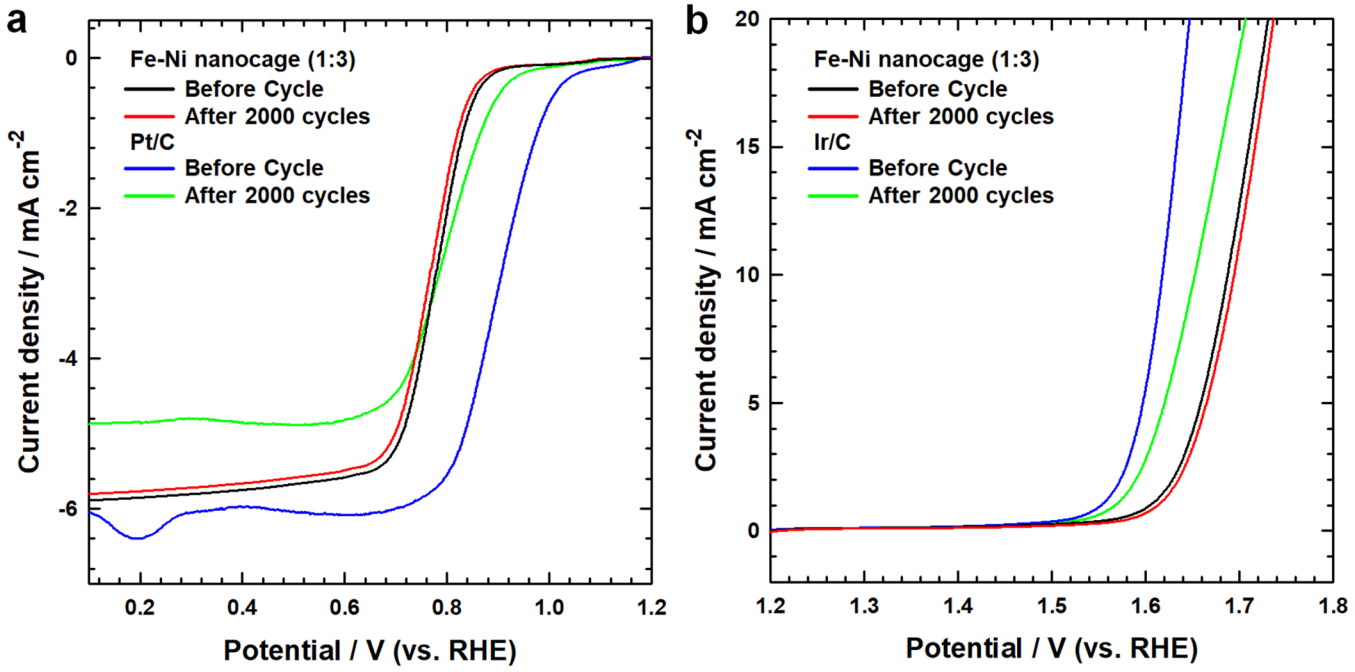

Figure 6. (a) ORR LSV curves of an Fe−Ni nanocage (1:3) and a commercial noble metal initially and after fast 2000 CV cycles. (b) OER LSV curves of an Fe−Ni nanocage (1:3) initially and after fast 2000 CV cycles.

in an LSV curve potential range from 0.9 to 0.5 V (vs RHE) and from 1.3 to 1.7 V (vs RHE), respectively. After 2000 cycles, commercial noble metal Pt/C and Ir/C showed an obvious decrease in their catalytic performance. In comparison, a very slight but negligible shifted potential and low current densities were observed for the Fe−Ni nanocage (1:3) in the ORR and OER durability tests, revealing that the Fe−Ni nanocage has a robust durability for alkaline electrolytes.

3. CONCLUSION

To use catalysts at the air−electrode interface of a metal−air battery, ORR and OER bifunctional performances are needed. We introduce a synergistic strategy for a bifunctional catalyst. First, we formed the hollow structure using a hydrogen bubble gas as a template for reduction. The materials were aggregated with a liquid−gas interface in a hydrogen bubble, with a simultaneously active inner cavity and outer shell. Consequently, the catalyst has a high active area and an outstanding catalytic performance. Second, we generated the electron transfer phenomenon using a doped nitrogen source. Nitrogen has a high electronegativity, causing metal cations to be deprived of electrons. Accordingly, the metal cation activity was accelerated by the nitrogen source, which is referred to as the "ensemble effect". The catalyst produced in this study exhibits excellent bifunctional properties and an excellent durability compared to the noble metals (platinum and iridium). This result provides a new strategy to develop high-performance unprecedented bifunctional catalysts.

■ ASSOCIATED CONTENT

Supporting Information

The Supporting Information is available free of charge at https://pubs.acs.org/doi/10.1021/acs.inorgchem.1c00782.

Synthesis procedures, characterization methods, additional TEM images, XPS spectra, and electrochemical performances (PDF)

■ AUTHOR INFORMATION

Corresponding Author

Jooheon Kim − *School of Chemical Engineering and Materials Science, Chung-Ang University, Seoul 06974, Republic of Korea; Department of Advanced Materials Engineering, Chung-Ang University, Anseong 17546, Republic of Korea;* orcid.org/0000-0002-6644-7791; Email: jooheonkim@cau.ac.kr

Authors

Taeoh Kang − *School of Chemical Engineering and Materials Science, Chung-Ang University, Seoul 06974, Republic of Korea*

Kwanwoo Kim − *School of Chemical Engineering and Materials Science, Chung-Ang University, Seoul 06974, Republic of Korea*

Complete contact information is available at: https://pubs.acs.org/10.1021/acs.inorgchem.1c00782

Notes

The authors declare no competing financial interest.

■ ACKNOWLEDGMENTS

This research was supported by the National Research Foundation of Korea (NRF) grant funded by the Korean government (MSIT) (2020R1A2C2010445).

■ REFERENCES

(1) Kim, M.; Ju, H.; Kim, J. Single crystalline Bi2Ru2O7 pyrochlore oxide nanoparticles as efficient bifunctional oxygen electrocatalyst for hybrid Na-air batteries. *Chem. Eng. J.* **2019**, *358*, 11−19.

(2) Kim, M.; Ju, H.; Kim, J. Highly efficient bifunctional catalytic activity of bismuth rhodium oxide pyrochlore through tuning the covalent character for rechargeable aqueous Na−air batteries. *J. Mater. Chem. A* **2018**, *6*, 8523−8530.

(3) Zhao, Z.; Yuan, Z.; Fang, Z.; Jian, J.; Li, J.; Yang, M.; Mo, C.; Zhang, Y.; Hu, X.; Li, P.; Wang, S.; Hong, W.; Zheng, Z.; Ouyang, G.;

Chen, X.; Yu, D. In Situ Activating Strategy to Significantly Boost Oxygen Electrocatalysis of Commercial Carbon Cloth for Flexible and Rechargeable Zn-Air Batteries. *Adv. Sci.* **2018**, *5*, 1800760.
(4) Xu, Q.; Jiang, H.; Li, Y.; Liang, D.; Hu, Y.; Li, C. In-situ enriching active sites on co-doped Fe-Co4N@N-C nanosheet array as air cathode for flexible rechargeable Zn-air batteries. *Appl. Catal., B* **2019**, *256*, 117893.
(5) Meng, F.; Zhong, H.; Bao, D.; Yan, J.; Zhang, X. In Situ Coupling of Strung Co4N and Intertwined N-C Fibers toward Free-Standing Bifunctional Cathode for Robust Efficient, and Flexible Zn-Air Batteries. *J. Am. Chem. Soc.* **2016**, *138*, 10226−31.
(6) Peng, W.; Wang, Y.; Yang, X.; Mao, L.; Jin, J.; Yang, S.; Fu, K.; Li, G. Co9S8 nanoparticles embedded in multiple doped and electrospun hollow carbon nanofibers as bifunctional oxygen electrocatalysts for rechargeable zinc-air battery. *Appl. Catal., B* **2020**, *268*, 118437.
(7) Ou, H.; Wang, D.; Li, Y. How to select effective electrocatalysts: Nano or single atom? *Nano Select* **2021**, *2*, 492−511.
(8) Kraytsberg, A.; Ein-Eli, Y. The impact of nano-scaled materials on advanced metal−air battery systems. *Nano Energy* **2013**, *2*, 468−480.
(9) Kim, M.; Ju, H.; Kim, J. Dihydrogen phosphate ion functionalized nanocrystalline thallium ruthenium oxide pyrochlore as a bifunctional electrocatalyst for aqueous Na-air batteries. *Appl. Catal., B* **2019**, *245*, 29−39.
(10) Higgins, D.; Chen, Z.; Lee, D. U.; Chen, Z. Activated and nitrogen-doped exfoliated graphene as air electrodes for metal−air battery applications. *J. Mater. Chem. A* **2013**, *1*, 2639.
(11) Cui, Z.; Li, Y.; Fu, G.; Li, X.; Goodenough, J. B. Robust Fe3Mo3 C Supported IrMn Clusters as Highly Efficient Bifunctional Air Electrode for Metal-Air Battery. *Adv. Mater.* **2017**, *29*, 1702385.
(12) Cui, Z.; Fu, G.; Li, Y.; Goodenough, J. B. Ni3 FeN-Supported Fe3 Pt Intermetallic Nanoalloy as a High-Performance Bifunctional Catalyst for Metal-Air Batteries. *Angew. Chem., Int. Ed.* **2017**, *56*, 9901−9905.
(13) Hardin, W. G.; Slanac, D. A.; Wang, X.; Dai, S.; Johnston, K. P.; Stevenson, K. J. Highly Active, Nonprecious Metal Perovskite Electrocatalysts for Bifunctional Metal-Air Battery Electrodes. *J. Phys. Chem. Lett.* **2013**, *4*, 1254−9.
(14) Chen, Z.; Yu, A.; Higgins, D.; Li, H.; Wang, H.; Chen, Z. Highly active and durable core-corona structured bifunctional catalyst for rechargeable metal-air battery application. *Nano Lett.* **2012**, *12*, 1946−52.
(15) Wei, L.; Ang, E. H.; Yang, Y.; Qin, Y.; Zhang, Y.; Ye, M.; Liu, Q.; Li, C. C. Recent advances of transition metal based bifunctional electrocatalysts for rechargeable zinc-air batteries. *J. Power Sources* **2020**, *477*, 228696.
(16) Gao, R.; Zhang, Q.; Soyekwo, F.; Lin, C.; Lv, R.; Qu, Y.; Chen, M.; Zhu, A.; Liu, Q. Novel amorphous nickel sulfide@CoS double-shelled polyhedral nanocages for supercapacitor electrode materials with superior electrochemical properties. *Electrochim. Acta* **2017**, *237*, 94−101.
(17) Oh, T.; Kim, K.; Kim, J. Controllable active sites and facile synthesis of cobalt nanoparticle embedded in nitrogen and sulfur co-doped carbon nanotubes as efficient bifunctional electrocatalysts for oxygen reduction and evolution reactions. *J. Energy Chem.* **2019**, *38*, 60−67.
(18) Hall, J. W.; Membreno, N.; Wu, J.; Celio, H.; Jones, R. A.; Stevenson, K. J. Low-temperature synthesis of amorphous FeP2 and its use as anodes for Li ion batteries. *J. Am. Chem. Soc.* **2012**, *134*, 5532−5.
(19) Kim, J.; Kim, H.; Kim, S.-K.; Ahn, S. H. Electrodeposited amorphous Co−P−B ternary catalyst for hydrogen evolution reaction. *J. Mater. Chem. A* **2018**, *6*, 6282−6288.
(20) Kim, K.; Kim, Y.; Kim, J. Enhanced cathodic catalytic activity of an N-doped micropore structure obtained through the six-coordinate bond of an EDTA-Ce composite for the oxygen reduction reaction. *Appl. Surf. Sci.* **2020**, *505*, 144418.
(21) Oh, T.; Kim, M.; Park, D.; Kim, J. Synergistic interaction and controllable active sites of nitrogen and sulfur co-doping into mesoporous carbon sphere for high performance oxygen reduction electrocatalysts. *Appl. Surf. Sci.* **2018**, *440*, 627−636.
(22) Goh, F. W. T.; Liu, Z.; Ge, X.; Zong, Y.; Du, G.; Hor, T. S. A. Ag nanoparticle-modified MnO2 nanorods catalyst for use as an air electrode in zinc−air battery. *Electrochim. Acta* **2013**, *114*, 598−604.
(23) Chunduri, A.; Gupta, S.; Bapat, O.; Bhide, A.; Fernandes, R.; Patel, M. K.; Bambole, V.; Miotello, A.; Patel, N. A unique amorphous cobalt-phosphide-boride bifunctional electrocatalyst for enhanced alkaline water-splitting. *Appl. Catal., B* **2019**, *259*, 118051.
(24) Ren, H.; Sun, X.; Du, C.; Zhao, J.; Liu, D.; Fang, W.; Kumar, S.; Chua, R.; Meng, S.; Kidkhunthod, P.; Song, L.; Li, S.; Madhavi, S.; Yan, Q. Amorphous Fe-Ni-P-B-O Nanocages as Efficient Electrocatalysts for Oxygen Evolution Reaction. *ACS Nano* **2019**, *13*, 12969−12979.
(25) Lu, X. F.; Chen, Y.; Wang, S.; Gao, S.; Lou, X. W. D. Interfacing Manganese Oxide and Cobalt in Porous Graphitic Carbon Polyhedrons Boosts Oxygen Electrocatalysis for Zn-Air Batteries. *Adv. Mater.* **2019**, *31*, No. 1902339.
(26) Zhang, H.; Qiao, H.; Wang, H.; Zhou, N.; Chen, J.; Tang, Y.; Li, J.; Huang, C. Nickel cobalt oxide/carbon nanotubes hybrid as a high-performance electrocatalyst for metal/air battery. *Nanoscale* **2014**, *6*, 10235−42.
(27) Zhao, J.; He, Y.; Chen, Z.; Zheng, X.; Han, X.; Rao, D.; Zhong, C.; Hu, W.; Deng, Y. Engineering the Surface Metal Active Sites of Nickel Cobalt Oxide Nanoplates toward Enhanced Oxygen Electrocatalysis for Zn-Air Battery. *ACS Appl. Mater. Interfaces* **2019**, *11*, 4915−4921.
(28) Senthilkumar, B.; Irshad, A.; Barpanda, P. Cobalt and Nickel Phosphates as Multifunctional Air-Cathodes for Rechargeable Hybrid Sodium-Air Battery Applications. *ACS Appl. Mater. Interfaces* **2019**, *11*, 33811−33818.
(29) Zhong, G.; Li, S.; Xu, S.; Liao, W.; Fu, X.; Peng, F. Nickel Nanoparticles Encapsulated in Nitrogen-Doped Carbon Nanotubes as Excellent Bifunctional Oxygen Electrode for Fuel Cell and Metal−Air Battery. *ACS Sustainable Chem. Eng.* **2018**, *6*, 15108−15118.
(30) Guo, X.; Hu, X.; Wu, D.; Jing, C.; Liu, W.; Ren, Z.; Zhao, Q.; Jiang, X.; Xu, C.; Zhang, Y.; Hu, N. Tuning the Bifunctional Oxygen Electrocatalytic Properties of Core-Shell Co3O4@NiFe LDH Catalysts for Zn-Air Batteries: Effects of Interfacial Cation Valences. *ACS Appl. Mater. Interfaces* **2019**, *11*, 21506−21514.
(31) Wang, W.; Liu, Y.; Li, J.; Luo, J.; Fu, L.; Chen, S. NiFe LDH nanodots anchored on 3D macro/mesoporous carbon as a high-performance ORR/OER bifunctional electrocatalyst. *J. Mater. Chem. A* **2018**, *6*, 14299−14306.
(32) Naik, K. M.; Sampath, S. Two-step oxygen reduction on spinel NiFe2O4 catalyst: Rechargeable. *Electrochim. Acta* **2018**, *292*, 268−275.
(33) Han, J.; Meng, X.; Lu, L.; Wang, Z. L.; Sun, C. Triboelectric nanogenerators powered electrodepositing tri-functional electrocatalysts for water splitting and rechargeable zinc-air battery: A case of Pt nanoclusters on NiFe-LDH nanosheets. *Nano Energy* **2020**, *72*, 104669.
(34) Liu, J.; Zhu, D.; Ling, T.; Vasileff, A.; Qiao, S.-Z. S-NiFe2O4 ultra-small nanoparticle built nanosheets for efficient water splitting in alkaline and neutral pH. *Nano Energy* **2017**, *40*, 264−273.
(35) Fu, G.; Cui, Z.; Chen, Y.; Xu, L.; Tang, Y.; Goodenough, J. B. Hierarchically mesoporous nickel-iron nitride as a cost-efficient and highly durable electrocatalyst for Zn-air battery. *Nano Energy* **2017**, *39*, 77−85.
(36) Yang, Z.; Liang, X. Self-magnetic-attracted NixFe(1-x)@NixFe(1-x)O nanoparticles on nickel foam as highly active and stable electrocatalysts towards alkaline oxygen evolution reaction. *Nano Res.* **2020**, *13*, 461−466.
(37) Zhu, J.; Chen, Z.; Xie, M.; Lyu, Z.; Chi, M.; Mavrikakis, M.; Jin, W.; Xia, Y. Iridium-Based Cubic Nanocages with 1.1-nm-Thick Walls: A Highly Efficient and Durable Electrocatalyst for Water Oxidation in an Acidic Medium. *Angew. Chem., Int. Ed.* **2019**, *58*, 7244−7248.

https://doi.org/10.1021/acs.inorgchem.1c00782
Inorg. Chem. 2021, 60, 7490−7497

(38) Sivakumar, P.; Ramesh, R.; Ramanand, A.; Ponnusamy, S.; Muthamizhchelvan, C. Synthesis studies and growth mechanism of ferromagnetic NiFe2O4 nanosheet. *Appl. Surf. Sci.* **2012**, *258*, 6648−6652.
(39) Zhang, R. H.; Zhao, T. S.; Jiang, H. R.; Wu, M. C.; Zeng, L. V2O5-NiO composite nanowires: A novel and highly efficient carbon-free electrode for non-aqueous Li-air batteries operated in ambient air. *J. Power Sources* **2019**, *409*, 76−85.
(40) Zhang, B.; Liu, J.; Wang, J.; Ruan, Y.; Ji, X.; Xu, K.; Chen, C.; Wan, H.; Miao, L.; Jiang, J. Interface engineering: The Ni(OH) 2 /MoS 2 heterostructure for highly efficient alkaline hydrogen evolution. *Nano Energy* **2017**, *37*, 74−80.
(41) Zeng, J.; Song, T.; Lv, M.; Wang, T.; Qin, J.; Zeng, H. Plasmonic photocatalyst Au/g-C3N4/NiFe2O4 nanocomposites for enhanced visible-light-driven photocatalytic hydrogen evolution. *RSC Adv.* **2016**, *6*, 54964−54975.
(42) Lin, C.; Wang, D.; Jin, H.; Wang, P.; Chen, D.; Liu, B.; Mu, S. Construction of an iron and oxygen co-doped nickel phosphide based on MOF derivatives for highly efficient and long-enduring water splitting. *J. Mater. Chem. A* **2020**, *8*, 4570−4578.
(43) Wang, H.-Y.; Hsu, Y.-Y.; Chen, R.; Chan, T.-S.; Chen, H. M.; Liu, B. Ni3+-Induced Formation of Active NiOOH on the Spinel Ni-Co Oxide Surface for Efficient Oxygen Evolution Reaction. *Adv. Energy Mater.* **2015**, *5*, 1500091.
(44) Li, X.; Han, G. Q.; Liu, Y. R.; Dong, B.; Hu, W. H.; Shang, X.; Chai, Y. M.; Liu, C. G. NiSe@NiOOH Core-Shell Hyacinth-like Nanostructures on Nickel Foam Synthesized by in Situ Electrochemical Oxidation as an Efficient Electrocatalyst for the Oxygen Evolution Reaction. *ACS Appl. Mater. Interfaces* **2016**, *8*, 20057−66.
(45) Wu, K. R.; Hung, C. H. Characterization of N,C-codoped TiO2 films prepared by reactive DC magnetron sputtering. *Appl. Surf. Sci.* **2009**, *256*, 1595−1603.

https://doi.org/10.1021/acs.inorgchem.1c00782
Inorg. Chem. 2021, 60, 7490−7497